Achilles tendons of MRL/MpJ mice show scar-mediated healing after tenotomy

Ningfeng Tang[1], Divya S. Sivalingam[2], Kimberly Wilson[1], Mehari M. Weldemariam[3], Hongying Tian[1], Christoph D. Hart[2], Prishasai Ramnath[2], Jacob Glazier[2], Jie Jiang[1], Natalie Leong[1], Tao Lowe[2,4], Maureen A. Kane[3], Masahiro Iwamoto[1], Catherine K. Kuo[1,2*], Motomi Enomoto-Iwamoto[1*]

[1]Department of Orthopaedics, University of Maryland School of Medicine, Baltimore, Maryland, USA

[2]Fischell Department of Bioengineering, A. James Clark School of Engineering, University of Maryland, College Park, Maryland, USA

[3]Department of Pharmaceutical Sciences, University of Maryland School of Pharmacy, Baltimore, Maryland, USA

[4]Department of Oral and Maxillofacial Surgery, School of Dentistry, University of Maryland, Baltimore, Maryland, USA

[*]Corresponding Authors:

Contact corresponding author
Catherine K. Kuo
Fischell Department of Bioengineering
A. James Clark School of Engineering
University of Maryland
4108 A. James Clark Hall, 8278 Paint Branch Dr
College Park, MD 20742, USA
ckk@umd.edu

Motomi Enomoto-Iwamoto
Department of Orthopaedics
University of Maryland School of Medicine
670 W Baltimore St, HSFIII 7171
Baltimore, MD 21201, USA
Motomi.iwamoto@som.umaryland.edu

Key words: tendon, injury, C57BL/6J, MRL/MpJ, proteomics

Abstract

Tendon healing in Murphy Ross Large (MRL/MpJ) mice was examined using an Achilles tendon tenotomy model, a full transection model, compared to a patella focal injury model in which tendons in MRL/MpJ mice showed regenerative healing. After complete transection, the Achilles tendons of MRL/MpJ mice healed via scar formation, regardless of sex, as did C57BL/6J mice. Tensile testing found that mechanical properties of injured tendons of both MRL/MpJ female and male mice exhibited comparable levels to those of C57BL/6J female and male mice, respectively after 4 weeks of healing, which is during the remodeling phase. After 10 weeks of healing, injured tendons of MRL/MpJ mice possessed smaller heterotopic ossification volumes than those of C57BL/6J mice. Proteomics analysis revealed similar alterations to signaling pathways in injured tendons of MRL/MpJ and C57BL/6J male mice after 4 weeks of healing. However, among the altered pathways, actin cytoskeleton and integrin signaling pathways were two of the top pathways that were more prominently activated in C57BL/6J males than in MRL/MpJ males. These findings indicate that MRL/MpJ mice possess limited capacity to regenerate injured tendons after complete rupture, and that tenotomized Achilles tendons of MRL/MpJ male mice have lesser induction of heterotopic ossification and lower activation of the signaling pathways also induced with injury in C57BL/6J male mice.

1. Introduction

Tendons have limited repair capacity. Injured tendons do not usually regain their original levels of biological, structural, and mechanical characteristics, and instead can undergo chronic degeneration [1-5]. In contrast to embryonic and neonatal tendons [6,7], adult tendons heal via scar formation characterized by high cell density, disorganized cell arrangement, thin and randomly aligned collagen fibers, high vascularity, and mucoid matrix [5,8]. Scar formation inhibits recovery

61 of mechanical properties. Failure of full functional recovery may result in chronic tendon
62 disorders and re-rupture, leading to poor quality of life and work disability [5]. Murphy Roths
63 Large (MRL/MpJ) mice have strong repair capacity in musculoskeletal tissues including articular
64 cartilage, muscle, and bone [9]. MRL/MpJ mice also exhibit more regenerative healing of focal
65 injuries of the patellar tendon in adults, based on better recovery of mechanical properties and
66 improved extracellular matrix and cell alignment when compared to healing of the same injury in
67 C57BL/6 mice [10,11]. A flexor tendon injury model involving partial laceration has also shown that
68 MRL/MpJ tendons heal with reduced fibrotic adhesion [12].

69 Based on these compelling prior works, we were interested in investigating whether tendons in
70 MRL/MpJ mice undergo regenerative healing even in an Achilles tendon complete transection
71 model, which is different from the focal injury models previously used to study tendon repair in
72 MRL/MpJ mice [10-12]. Determining the molecular mechanism that supports the reparative ability
73 of the MRL/MpJ is crucial to develop new modalities to promote effective tendon healing, and
74 thus we also used proteomics analyses to examine which signaling pathways may be involved in
75 improved tendon repair by MRL/MpJ mice.

76 2. Materials and Methods

77 2.1. Mouse experiments

78 All animal studies were conducted with approval from the Institutional Animal Care and Use
79 Committee at the University of Maryland, Baltimore (0120007 and 1122006). Animals were
80 housed in a University Laboratory Animal Resources supervised animal facility with a 12-hour
81 light/dark cycle and controlled temperature of 22 ± 1ºC and humidity of 55 ± 5%. Animals were
82 provided hygienic animal bedding of wood shavings and cotton pads. The health status of each

animal was monitored throughout the experiments by investigators, animal veterinary technicians, and veterinarians, as per institutional guidelines. The mice were free of all viral, bacterial, and parasitic pathogens during the experimental schedule.

A complete transverse transection (tenotomy), without attempt at repair, was made at the midpoint of the left Achilles tendon in 12-week-old female and male C57BL/6J (#000646, The Jackson Laboratory, Bar Harbor, ME) and MRL/MpJ (#000486, The Jackson Laboratory) mice under anesthesia. The analgesic carprofen, 4.5 mg/Kg was administrated pre- and post-surgery. The mice receiving the tenotomy surgery were euthanized 4 or 10-weeks post-surgery, which was during the early and late remodeling phase, respectively. The right and left hind limbs were collected for histological analysis and mechanical tests. The mid-substance of Achilles tendons was snap frozen in liquid nitrogen and stored at -80°C until use. The criteria for animal exclusion during the experiment, determined prior to the experiment, were to exclude mice that received analgesics and/or antibiotics and/or were euthanized due to infection or distress. No mice were excluded in this study. No exclusion criteria were set for data points during the analysis. No data points were excluded. MRL/MpJ and C57BL/6J mice were maintained in the same location and compared, but randomization was not used and confounders were not controlled. A total of 109 mice were used: 3 female C57BL/6J, 3 male C57BL/6J, 3 female MRL/MpJ, and 3 male MRL/MpJ mice for histological examination at 4 weeks post- surgery; 8 female C57BL/6J, 5 female MRL/MpJ, 8 male C57BL/6J, and 7 female MRL/MpJ mice for mechanical testing at 4 weeks post-surgery; 5 male C57BL/6J, 5 male MRL/MpJ, 4 female C57BL/6J, and 3 female MRL/MpJ mice for μCT analysis at 10 weeks post-surgery; 18 uninjured male C57BL/6J mice (for 5 unique biological replicates), 10 injured male C57BL/6J mice (for 5 unique biological replicates), 10 uninjured male MRL/MpJ mice (for 4 unique

106 biological replicates), and 8 injured male MRL/MpJ mice (for 4 unique biological replicates) for
107 proteomics at 4-weeks post-surgery; and 3 C57BL/6J and 3 MRL/MpJ male mice for
108 immunoblotting at 4 weeks post-surgery. Healing ability comparisons between MRL/MpJ and
109 C57BL/6J mice were based on mechanical properties (primary outcome measure) and histology
110 (secondary outcome measure).

111 2.2. Histology

112 The hind limbs were fixed with 4% paraformaldehyde for 24 hours at 4°C and decalcified with
113 10% ethylenediaminetetraacetic acid at pH 7.2. Serial sagittal sections (5 µm) of the injured or
114 contralateral uninjured Achilles tendons were made. Sections were stained with hematoxylin-
115 eosin and picrosirius red. Hematoxylin-eosin staining images were captured using light
116 microscopy (BZX-700, Keyence, Tokyo, Japan). Picrosirius red staining images were captured
117 using polarized light microscopy (20X objective, ZEISS Axio Scan, Germany) [7,13-15].

118 2.3. Micro-computed tomography (microCT) analysis

119 Samples were scanned using a Skyscan 1172 microCT scanner (Bruker, Billerica, MA, USA)
120 while immersed in phosphate buffered saline without Ca^{2+} or Mg^{2+} (PBS). Specifically, images
121 were acquired using previously reported conditions [16]: 6.5 µm/pixel; 0.2 mm Al filter using a 55
122 kV X-ray source; resolution at 2 K with step rotation of 0.51; and two average frames using 360°
123 rotation. Image reconstruction was performed using NRecon software (Bruker). We manually
124 identified regions of heterotopic ossification by setting threshold between 80 and 255, for which
125 volume analyses were performed using CTAn software (Bruker). Rendering images were
126 obtained using CTVOX (Bruker).

127 2.4. Mass spectrometry-based proteomics

128 We collected tendon samples and stored them at -80 ºC until assay. Lysis buffer containing 5%
129 SDS (sodium dodecyl sulfate) and 50 mM triethylammonium bicarbonate (1 M, pH 8.0) was
130 added to tendons and the samples were then homogenized using bead beating with a Precellys
131 CK14 lysing kit (Bertin Corp., Rockville, MD). Next, protein extraction and digestion were
132 performed as described [17] using S-trap micro columns (ProtiFi, NY). Digested peptides were
133 quantified using a BCA assay kit (Thermo Fisher Scientific, 23275) to determine peptide
134 concentration. LC-MS/MS-based proteomic analysis was conducted on a nanoACQUITY Ultra-
135 Performance Liquid Chromatography system (Waters Corporation, Milford, MA USA) coupled
136 to an Orbitrap Fusion Lumos Tribrid mass spectrometer (Thermo Scientific, San Jose, CA USA).
137 Peptide separation was effected on a nanoACQUITY Ultra-Performance Liquid Chromatography
138 (UPLC) analytical column (BEH130 C18, 1.7 µm, 75 µm x 200 mm; Waters Corporation,
139 Milford, MA, USA) using a 185-min linear gradient with 3-40% acetonitrile and 0.1% formic
140 acid. Mass spectrometry conditions were as follows: Full MS scan resolution of 240,000,
141 precursor ions fragmentation by high-energy collisional dissociation of 35%, and a maximum
142 cycle time of 3 seconds. The resulting mass spectra were processed using Thermo Proteome
143 Discoverer ((PD, version 3.0.0.757), Thermo Fisher Scientific) and searched against a UniProt
144 mouse reference proteome (release 2024.03, 17180 entries) using Sequest HT algorithm. Search
145 parameters include carbamidomethylation of cysteines (+57.021 Da) as a static modification,
146 methionine oxidation (+15.995 Da) as a dynamic modification, precursor mass tolerance of 20
147 ppm, fragment mass tolerance of 0.5 Da, and trypsin as a digestion enzyme. Tryptic missed
148 cleavages were restricted to a maximum of two, with peptide lengths set between 6 and 144
149 residues. For protein quantification, the Minora feature detector, integrated in the PD, was used
150 as described previously [17]. To ensure high data quality, proteins were further filtered to a 1%

false discovery rate (FDR) threshold, calculated with the Percolator algorithm. Next, protein abundance values exported from PD were post-processed using Perseus software (version 1.6.14.0). Proteins with missing values were excluded to improve data quality. Differentially expressed proteins (DEPs) were identified using a two-tailed Student's t-test (adjusted p-value < 0.05). Ingenuity Pathway Analysis (IPA) software (Qiagen, Germantown, MD) was used to identify dysregulated pathways and biological processes. The data were deposited in the ProteomeXchange via the PRIDE database, with the project accession number PXD057712.

2.6. Mechanical Testing

Achilles tendons with calcanei were fine dissected to ensure removal of all musculature and surrounding soft tissue. Injured and contralateral uninjured tendons were hydrated in PBS immediately after dissection and throughout the course of mechanical testing. Prior to mechanical testing, the dissected tendons were suspended in a tube pinching the calcaneus with the lid and scanned using a Skyscan 1172 microCT scanner (Camera pixel size, 9.00; Rotation range, 360 deg; Image rotation, 3 deg; scanning time, about 9 mins). PBS was placed in the bottom of the tube to prevent the tendon from drying. The volume and length of the tendon were measured using CTAn software. The cross-sectional area (CSA) was then calculated as the ratio of volume to length. Mechanical testing was performed, as previously described [18], on a DMA850 dynamic mechanical analyzer (TA Instruments, New Castle, DE) with TRIOS Software. Tendons were gripped between the calcaneus and myotendinous junction and underwent a uniaxial tensile testing protocol consisting of a preload to 0.02 N, and then ramp to failure test at 0.1% strain per second. Mechanical (ultimate force, stiffness) and material (elastic modulus, ultimate stress, ultimate strain) properties were determined, as previously described [19].

2.7. Statistical analysis

Power analysis (G*Power v.3.1, Heinrich Heine Universität Düsseldorf, Germany) performed using experimental data, with power of 0.80 and significance level $\alpha=0.05$, determined that a minimum sample size of N=5 biological replicates (different mice) per experimental group was needed. Data was assumed to be drawn from a normally distributed population. Normality was analyzed by the Shapiro-Wilk test. Non-parametric tests were selected when the assumption of normality could not be met. Mechanical testing and heterotopic ossification results were analyzed using Prism 10 (10.6.0, Graphpad, San Diego, CA). Material and mechanical properties were compared between sexes, mouse strains, and uninjured and injured tendons using a one-way ANOVA with Tukey's post-hoc. Heterotopic ossification results were analyzed by Mann-Whitney or Kologorov-Smirnov test to identify differences between groups. The threshold for significance for all tests was set as $p<0.05$. The data met the assumptions of the statistical approach.

3. Results

3.1. Both C57BL/6J and MRL/MpJ mouse Achilles tendons presented with scar formation after tenotomy.

C57BL/6J and MRL/MpJ mice received unilateral tenotomy of the Achilles tendon. To investigate an early remodeling phase, we examined the recovery of extracellular matrix organization at 4 weeks after surgery. Sagittal sections of injured Achilles tendons from both female and male mice were acquired. Figure 1 shows sagittal sections of polarized images stained with picrosirius red from the distal calcaneal insertion (left, single arrow) to the proximal myotendinous junction (right, double arrow). Injured C57BL/6J tendons showed disorganized immature collagen fibers (Fig. 1A and 1E), compared to aligned collagen fibers in uninjured tendons of age- and sex-matched mice (Fig. 1B and 1F). Injured Achilles tendons of both female

197 and male MRL/MpJ mice also showed disorganized immature collagen fibers with polarized
198 imaging (Fig. 1C and 1G), in contrast to uninjured tendons (Fig. 1D and 1H). The hematoxylin
199 and eosin-stained sections of injured tendons presented as scar tissue rich in fibroblasts and
200 blood vessels (Fig. 2A-2H), whereas uninjured Achilles tendons from age-, sex-, and strain-
201 matched mice appeared dense with extracellular matrix and aligned tenocytes. (Fig. 2I-2L).

202 3.2. Recovery of material and mechanical properties of injured MRL/MpJ Achilles tendons were
203 comparable to that of C57BL/6J Achilles tendons.

204 Injured Achilles tendons of female and male MRL/MpJ mice possessed lower stiffness, elastic
205 modulus, ultimate load, and ultimate stress, but greater ultimate strain compared to their
206 corresponding uninjured MRL/MpJ Achilles tendons (Fig. 3, S1, and S2). Similarly, injured
207 female and male C57BL/6J tendon stiffness, elastic modulus, ultimate load, and ultimate stress
208 were lower, whereas ultimate strain was higher, than their corresponding uninjured Achilles
209 tendons (Fig. 3 and S2). In addition, the injury-induced changes in stiffness, elastic modulus,
210 ultimate load, ultimate stress, and ultimate strain were similar between MRL/MpJ and C57BL/6J
211 tendons (Fig. 3 and S2), suggesting that recovery of material and mechanical properties of
212 injured MRL/MpJ tendons is comparable to that of injured C57BL/6J tendons. Further, sex-
213 specific differences in material and mechanical properties in either injured or uninjured tendons
214 of either strain were not found (Fig. 3 and S2).

215 3.3. MRL/MpJ Achilles tendons possessed lower volume of heterotopic ossification compared to
216 C57BL/6J Achilles tendons.

217 The mouse Achilles tendon tenotomy model has been studied as a heterotopic ossification model
218 based on the established phenomenon of chondroid degeneration followed by ectopic bone

formation in injured Achilles tendons by later timepoints of healing [20]. Injury-induced heterotopic ossification was analyzed by microCT scan ten weeks after surgery, the time when heterotopic ossification is evident in this model [20]. Injury induced heterotopic ossification in both C57BL/6J and MRL/MpJ Achilles tendons (Fig. 4A). The total volume of heterotopic ossified regions was smaller in MRL/MpJ male tendons than that in C57BL/6J male tendons (Fig. 4B, left). Combining male and female results also revealed significantly smaller volumes of heterotopic ossification in MRL/MpJ mice (Fig. 4B, right).

3.4. Activation of actin cytoskeleton and integrin signaling pathways was less pronounced in MRL/MpJ male Achilles injured tendons.

We performed proteomic analysis of the samples obtained from C57BL/6J and MRL/MpJ male injured and uninjured Achilles tendons. Differentially expressed proteins (DEPs) were identified using a two-tailed Student's t-test with a criterion of adjusted p-value < 0.05 (Fig. 5A). We found that 538 proteins and 595 proteins were up-regulated in C57BL/6J injured tendons and MRL/MpJ injured tendons, respectively, compared with the mouse strain-matched uninjured tendons, whereas 79 proteins and 54 proteins were down-regulated in C57BL/6J injured tendons and MRL/MpJ injured tendons, respectively. Comparison between C57BL/6J and MRL/MpJ male injured tendons showed that 335 proteins were up-regulated and 70 proteins were down-regulated in C57BL/6J injured tendons compared to MRL/MpJ injured tendons. In spite of differences in DEPs between C57BL/6J and MRL/MpJ samples, based on IPA, C57BL/6J and MRL/MpJ injured tendons revealed similar alterations of the canonical pathways relative to their corresponding uninjured tendons (Supplementary Table 1). When the top 100 pathways were compared between C57BL/6J and MRL/MpJ groups, the top 50 pathways overlapped completely, and exhibited differences only in the rank order (common pathways in

242 Supplementary Table 1, highlighted). Both C57BL/6J and MRL/MpJ activated the same top 5
243 pathways with positive z-scores, including actin cytoskeleton signaling and integrin signaling
244 pathways relative to respective uninjured groups (Fig. 5B). Interestingly, actin cytoskeleton
245 signaling and integrin signaling pathways were also listed amongst the top 5 pathways in
246 C57BL/6J injured tendons relative to MRL/MpJ injured tendons (Fig. 5C, z-score 2.294 and
247 2.985, respectively). This was also observed in C57BL/6J uninjured tendons relative to
248 MRL/MpJ uninjured tendons (Fig. 5C).

249 4. Discussion

250 Our results indicate that tenotomized Achilles tendons of MRL/MpJ mice heal similarly as those
251 of C57BL/6J mice, but with reduced heterotopic ossification than in C57BL/6J tendons by late
252 stages of healing. Further, the injured tendons in MRL/MpJ male mice had lesser activation of
253 actin cytoskeleton and integrin signaling pathways. These findings demonstrate MRL/MpJ mice
254 possess limited capacity to regenerate injured tendons after complete rupture, but with reduced
255 heterotopic ossification and activation of some molecular signaling pathways during tendon
256 healing, such as cytoskeleton and integrin signaling, compared to C57BL/6J mice.

257 Superior healing by the MRL/MpJ mouse has been previously reported for patellar tendon
258 injuries [21]. After a 0.75 to 1 mm full-thickness focal defect in the patellar tendon, MRL/MpJ
259 mice exhibit greater recovery of mechanical properties [10] and superior extracellular matrix
260 realignment [21], compared to C57BL/6J mice. MRL/MpJ mice have also demonstrated improved
261 recovery of mechanical strength after full-length and full-thickness central patellar tendon
262 injuries [11], although pathology of their healing process has not been reported. In the Achilles
263 tendon tenotomy model that we used here, C57BL/6J mice exhibit scar-mediated healing [20].
264 Neo-tissue forms in the gap of the transected tendon in the first week after surgery, and the newly

formed tissue gradually remodels over the next several weeks, with a decrease in cell density and increase in sagittal alignment of cells [20]. However, the remodeled tissue still contains poorly aligned, thin collagen fibers [8] and undergoes chondroid degeneration and progressive heterotopic ossification 8 to 10 weeks after injury [20,22]. Here, we found that after complete transection, MRL/MpJ injured Achilles tendons demonstrated fibrotic healing as observed in C57BL/6J mice, but the ectopic ossified mass was smaller in MRL/MpJ mice than in C57BL/6J mice. Furthermore, by 4 weeks of healing, there was no difference in the extent of recovery of mechanical properties between MRL/MpJ mice and C57Bl/6J mice regardless of sex. It appears that completely transected Achilles tendons in MRL/MpJ mice undergo scar-mediated healing, and do not have superior healing ability compared to C57BL/6J mice. However, additional investigations are needed, including quantitative analysis of histology, as well as mechanical testing and histological analysis at later stages.

In this study, we used a tendon injury model of complete transection of the Achilles tendon whereas previous studies have used a focal injury model of the patellar tendon that has shown regenerative healing [10,21,23]. Considering the many differences between the tenotomized Achilles tendon injury model versus the patella tendon focal injury model, such as tendon type, injury size, and instability of injury site by motion, it is not possible to make generalized conclusions about the healing ability of MRL/MpJ tendons. In addition, the Achilles tendon injury model has limitations, including the development of ectopic bone formation, and the lack of maintaining the tendon ends in apposition following transection and during healing. Nevertheless, our results suggest that the regenerative capacity of tendons in the MRL/MpJ mouse may be limited depending on the type of injury as well as the anatomical location of the tendon. It has been suggested by others that MRL/MpJ regenerative healing extent depends on injury type or

288 severity [11]. Failure by the MRL/MpJ mouse to fully regenerate after injury has been
289 demonstrated in other injured tissues, including the heart after ischemia-reperfusion injury [9,24],
290 the skin after excisional injury [25], and articular cartilage after full-thickness injury [26]. Here, we
291 did not observe sex-specific differences in elastic modulus, ultimate stress, and ultimate strain of
292 injured Achilles tendons 4 weeks after injury. This is consistent with previous findings that
293 MRL/MpJ patellar tendon focal defects do not exhibit sex-specific differences in mechanical or
294 material properties [27]. However, male MRL/MpJ mice exhibit superior healing of articular
295 cartilage full-thickness injuries compared to female MRL/MpJ mice [26]. Interestingly, the
296 heterotopic calcified volume in the injured Achilles tendons trended larger in males than in
297 females, regardless of strain: 0.838+/- 0.600 mm^3 versus 1.648 +/- 0.122 mm^3 for C57BL/6J
298 female versus male mice, respectively; and 0.209 +/-0.189 mm^3 versus 0.588 +/- 0.348 mm^3 for
299 MRL/MpJ female versus male mice, respectively. In injured mouse Achilles tendons, heterotopic
300 bone formation occurs via endochondral ossification at late healing stage [20]. Taken together, male
301 MRL/MpJ mice may have a stronger ability to generate cartilage tissue than female mice,
302 resulting in the induction of larger volumes of cartilage-mediated ectopic bone in healing
303 tendons.
304 To examine the molecular mechanisms involved in tendon healing, we performed proteomics
305 analysis of injured tendons during the remodeling phase, 4 weeks after injury, because previous
306 studies investigated the differences in the cells, matrix proteins, and signaling molecules between
307 MRL/MpJ and C57BL/6J mouse patellar tendons during the inflammation and proliferation
308 phases of early healing [10-12,21,23]. Here, the altered signaling pathways in injured tendons during
309 the remodeling phase were similar between MRL/MpJ and C57BL/6J mice, suggesting that in
310 both strains, similar signaling pathways are altered upon injury, and similar molecular

311 mechanisms are involved in scar formation and matrix remodeling. Intriguingly, we found that
312 the MRL/MpJ male tendons showed less activation of the actin cytoskeleton and integrin
313 signaling pathways than the C57BL/6J male tendons. These pathways govern cell adhesion,
314 migration, proliferation, and matrix synthesis and organization [28]. Upregulation of these
315 pathways in response to injury is expected and is likely purposeful, especially during early
316 healing phases after injury because inflammation and angiogenesis occur during the
317 inflammatory phase, and reparative cells such as tendon progenitors and myofibroblasts migrate
318 into and proliferate in the injured site during the proliferation phase [29]. Actin cytoskeletal
319 proteins and integrin adhesion complexes are essential molecules in regulation of migration,
320 differentiation, matrix synthesis, and organization of myofibroblasts [30]. It is of note that early
321 upregulation of integrins and cellular adhesion genes have also been implicated in superior
322 MRL/MpJ patellar tendon focal defect healing [27]. Higher expression of *Itgb1* during the first 7
323 days post-injury was postulated to lead to improved cell and matrix alignment in MRL/MpJ
324 healing patellar tendons, compared to C57BL/6J tendons. In contrast, during the remodeling
325 phase, higher activity of these signaling pathways may be caused by or be associated with higher
326 activity of fibrous tissue formation, leading to greater inhibition of structural recovery of
327 collagen fibers and functional recovery of mechanical properties in C57BL/6J mice.
328 Future studies should investigate the differences in the tendon healing processes between
329 MRL/MpJ and C57BL/6J mice over a longer period in this tenotomy injury model. In particular,
330 material property characterizations – including elastic modulus, ultimate strength, and collagen
331 crosslink density – should be determined after additional longer healing durations to more fully
332 evaluate long-term recovery of function and restoration of tissue quality. Quantitative
333 assessments of histological characterizations, including fibrillar collagen density and alignment,

cell and nuclear morphology, and integrin binding are needed to better inform the extent of scarless healing in MRL/MpJ mice. Identification of specific molecules that regulate the increased activity of the actin cytoskeleton and integrin signaling pathways and validation of their role in injured C57BL/6J tendon healing is also needed. Despite the unexpected discovery of limited MRL/MpJ tendon healing capacity observed in this study, these data suggest that lower activity of the actin cytoskeleton and integrin signaling pathways may be associated with a lower degree of heterotopic ossification. Complementing our current data with future proteomic characterizations of healing MRL/MpJ versus C57BL/6J female Achilles tendons, along with validation of specific protein targets, will provide more comprehensive insight into the sex-specific MRL/MpJ regenerative healing capacity for tendon injuries.

Contributions: CKK and MEI designed the experiments. NT, KW, MW, HT, CDH, PR, and MEI conducted experiments; NT, DSS, JJ, NL, MAK, CKK, and MEI evaluated the results; and CKK and MEI prepared the manuscript. All authors have read and approved the final submitted manuscript.

Funding: This work is supported by NIH / National Institute of Arthritis and Musculoskeletal and Skin Diseases Grant/Award Numbers: R01AR070099 (MEI), R21AR080996 (MEI), R01AR072886 (CKK), and R21AR077756 (CKK), University of Maryland Baltimore, Institute for Clinical &Translational Research Pilot grant at #457 (MEI).

Acknowledgments: We thank D. Muthusamy and E. Mirdamadi for assistance with the DMA850.

356 References

357 [1] Sharma P, Maffulli N. Tendon injury and tendinopathy: healing and repair. J Bone Joint
358 Surg Am. Jan 2005;87(1):187-202. doi:87/1/187 [pii]

359 10.2106/JBJS.D.01850

360 [2] Rees JD, Wilson AM, Wolman RL. Current concepts in the management of tendon
361 disorders. Rheumatology (Oxford). May 2006;45(5):508-21. doi:kel046 [pii]

362 10.1093/rheumatology/kel046

363 [3] Aslan H, Kimelman-Bleich N, Pelled G, Gazit D. Molecular targets for tendon
364 neoformation. J Clin Invest. Feb 2008;118(2):439-44. doi:10.1172/JCI33944

365 [4] Nourissat G, Berenbaum F, Duprez D. Tendon injury: from biology to tendon repair. Nat
366 Rev Rheumatol. Apr 2015;11(4):223-33. doi:10.1038/nrrheum.2015.26

367 [5] Galatz LM, Gerstenfeld L, Heber-Katz E, Rodeo SA. Tendon regeneration and scar
368 formation: The concept of scarless healing. J Orthop Res. Jun 2015;33(6):823-31.
369 doi:10.1002/jor.22853

370 [6] Howell K, Chien C, Bell R, et al. Novel Model of Tendon Regeneration Reveals Distinct
371 Cell Mechanisms Underlying Regenerative and Fibrotic Tendon Healing. Sci Rep. Mar 23
372 2017;7:45238. doi:10.1038/srep45238

373 [7] Nguyen PK, Hart C, Hall K, Holt I, Kuo CK. Establishing in vivo and ex vivo chick
374 embryo models to investigate fetal tendon healing. Sci Rep. Jun 13 2023;13(1):9600.
375 doi:10.1038/s41598-023-35408-w

376 [8] Izumi S, Oichi T, Shetye SS, et al. Inhibition of glucose use improves structural recovery
377 of injured Achilles tendon in mice. J Orthop Res. Jun 2022;40(6):1409-1419.
378 doi:10.1002/jor.25176

379 [9] Rai MF, Sandell LJ. Regeneration of articular cartilage in healer and non-healer mice.
380 Matrix Biol. Oct 2014;39:50-5. doi:10.1016/j.matbio.2014.08.011

381 [10] George NS, Bell R, Paredes JJ, Taub PJ, Andarawis-Puri N. Superior mechanical
382 recovery in male and female MRL/MpJ tendons is associated with a unique genetic profile. J
383 Orthop Res. Apr 30 2020;39(6):1344-1354. doi:10.1002/jor.24705

384 [11] Lalley AL, Dyment NA, Kazemi N, et al. Improved biomechanical and biological
385 outcomes in the MRL/MpJ murine strain following a full-length patellar tendon injury. J Orthop
386 Res. Nov 2015;33(11):1693-703. doi:10.1002/jor.22928

387 [12] Kallenbach JG, Freeberg MAT, Abplanalp D, et al. Altered TGFB1 regulated pathways
388 promote accelerated tendon healing in the superhealer MRL/MpJ mouse. Sci Rep. Feb 22
389 2022;12(1):3026. doi:10.1038/s41598-022-07124-4

390 [13] Marturano JE, Arena JD, Schiller ZA, Georgakoudi I, Kuo CK. Characterization of
391 mechanical and biochemical properties of developing embryonic tendon. Proc Natl Acad Sci U S
392 A. Apr 16 2013;110(16):6370-5. doi:10.1073/pnas.1300135110

393 [14] Nguyen PK, Jana A, Huang C, et al. Tendon mechanical properties are enhanced via
394 recombinant lysyl oxidase treatment. Front Bioeng Biotechnol. 2022;10:945639.
395 doi:10.3389/fbioe.2022.945639

396 [15] Korntner SH, Jana A, Kinnard E, et al. Craniofacial tendon development-Characterization
397 of extracellular matrix morphology and spatiotemporal protein distribution. Front Cell Dev Biol.
398 2022;10:944126. doi:10.3389/fcell.2022.944126

399 [16] Garcia SA, Wilson K, Tang N, et al. Analysis of the Actions of RARγ Agonists on
400 Growing Osteochondromas in a Mouse Model. Int J Mol Sci. Jul 11 2024;25(14).
401 doi:10.3390/ijms25147610

402 [17] Weldemariam MM, Sudhir PR, Woo J, Zhang Q. Effects of multiple stressors on
403 pancreatic human islets proteome reveal new insights into the pathways involved. Proteomics.
404 Oct 2023;23(19):e2300022. doi:10.1002/pmic.202300022

405 [18] Kurtaliaj I, Golman M, Abraham AC, Thomopoulos S. Biomechanical Testing of Murine
406 Tendons. J Vis Exp. Oct 15 2019;(152)doi:10.3791/60280

407 [19] Navarro J, Korcari A, Nguyen P, et al. Method development and characterization of chick
408 embryo tendon mechanical properties. J Biomech. Mar 2022;133:110970.
409 doi:10.1016/j.jbiomech.2022.110970

410 [20] Asai S, Otsuru S, Candela ME, et al. Tendon progenitor cells in injured tendons have
411 strong chondrogenic potential: the CD105-negative subpopulation induces chondrogenic
412 degeneration. Stem Cells. Dec 2014;32(12):3266-77. doi:10.1002/stem.1847

413 [21] Paredes J, Shiovitz DA, Andarawis-Puri N. Uncorrelated healing response of tendon and
414 ear injuries in MRL highlight a role for the local tendon environment in driving scarless healing.
415 Connect Tissue Res. Sep 2018;59(5):472-482. doi:10.1080/03008207.2018.1485665

416 [22] Zhang K, Asai S, Hast MW, et al. Tendon mineralization is progressive and associated
417 with deterioration of tendon biomechanical properties, and requires BMP-Smad signaling in the
418 mouse Achilles tendon injury model. Matrix Biol. May-Jul 2016;52-54:315-24.
419 doi:10.1016/j.matbio.2016.01.015

420 [23] Paredes J, Pekmezian A, Andarawis-Puri N. MRL/MpJ tendon matrix-derived therapeutic
421 promotes improved healing outcomes in scar-mediated canonical tendon healing. J Orthop Res.
422 May 22 2020;39(7):1548-1560. doi:10.1002/jor.24754

423 [24] Abdullah I, Lepore JJ, Epstein JA, Parmacek MS, Gruber PJ. MRL mice fail to heal the
424 heart in response to ischemia-reperfusion injury. Wound Repair Regen. 2005;13(2):205-8.
425 doi:10.1111/j.1067-1927.2005.130212.x

426 [25] Colwell AS, Krummel TM, Kong W, Longaker MT, Lorenz HP. Skin wounds in the
427 MRL/MPJ mouse heal with scar. Wound Repair Regen. Jan-Feb 2006;14(1):81-90.
428 doi:10.1111/j.1524-475X.2005.00092.x

429 [26] Fitzgerald J, Rich C, Burkhardt D, Allen J, Herzka AS, Little CB. Evidence for articular
430 cartilage regeneration in MRL/MpJ mice. Osteoarthritis Cartilage. Nov 2008;16(11):1319-26.
431 doi:10.1016/j.joca.2008.03.014

432 [27] George NS, Bell R, Paredes JJ, Taub PJ, Andarawis-Puri N. Superior mechanical
433 recovery in male and female MRL/MpJ tendons is associated with a unique genetic profile. J
434 Orthop Res. Jun 2021;39(6):1344-1354. doi:10.1002/jor.24705

435 [28] Hynes RO. Integrins: bidirectional, allosteric signaling machines. Cell. Sep 20
436 2002;110(6):673-87. doi:S0092867402009716 [pii]

437 [29] Thomopoulos S, Parks WC, Rifkin DB, Derwin KA. Mechanisms of tendon injury and
438 repair. J Orthop Res. Jun 2015;33(6):832-9. doi:10.1002/jor.22806

439 [30] Younesi FS, Hinz B. The Myofibroblast Fate of Therapeutic Mesenchymal Stromal Cells:
440 Regeneration, Repair, or Despair? Int J Mol Sci. Aug 9 2024;25(16):8712.
441 doi:10.3390/ijms25168712

442 Figure Legends

443 Fig. 1. Comparison of picrosirius red (PSR)-stained sections of injured tendons between
444 C57BL/6J and MRL/MpJ mice. A complete transverse transection was made at the midpoint of
445 the left Achilles tendon in 12-week-old female and male C57BL/6J (A, B, E, and F) and
446 MRL/MpJ (C, D, G, and H) mice (n=3 per sex and strain). Sagittal sections of the injured (A, C,
447 E, and G) and contralateral uninjured (B, D, F, and H) Achilles tendons four weeks after surgery
448 were stained with PSR. Bar represents 1.5 mm. Arrow and double arrow show distal calcaneal
449 insertion and proximal myotendinous junction of the Achilles tendon, respectively.

450 Fig. 2. Comparison of hematoxylin-eosin-stained sections of injured tendons between C57BL/6J
451 and MRL/MpJ mice. A complete transverse transection was made at the midpoint of the left
452 Achilles tendon in 12-week-old female and male C57BL/6J (A-D, I and J) and MRL/MpJ (E-H,
453 K and L) mice (n=3 per sex and strain). Sagittal sections of the injured (A-H) and contralateral
454 uninjured (I-L) Achilles tendons four weeks after surgery were stained with hematoxylin-eosin
455 (HE).

456

457 Fig. 3. Comparison of biomechanical properties of injured tendons between C57BL/6J and
458 MRL/MpJ mice. A complete transverse transection was made at the midpoint of the left Achilles

tendon in 12-week-old female (circles; F) and male (squares; M) C57BL/6J (blue; n=7 for female and n=8 for male) and MRL/MpJ (red; n=5 for female and n=7 for male) mice. Four weeks after surgery, injured (Inj; left limb) and contralateral uninjured (Uninj; right limb) limbs were harvested. Dissected tendons were mechanically assessed using tensile testing. (A) Cross-sectional area (CSA), (B) stiffness, (C) ultimate load, (D) elastic modulus, (E) ultimate stress, and (F) ultimate strain were compared between uninjured and injured tendons of C57BL/6J female (blue circles), MRL/MpJ female (red circles), C57BL/6J male (blue squares), and MRL/MpJ male (red squares). Data points represent individual biological replicates. For (A-F), p-values of statistically significant comparisons between uninjured and injured of the same sex and strain, between sexes of the same injury status and strain, and between strains of the same injury status and sex are shown. Averages and standard deviations of absolute values are summarized in Fig. S2 of Supplementary Material. (G-I) Injured values were normalized to average uninjured values of the respective group and (G) elastic modulus, (H) ultimate stress, and (I) ultimate strain were compared between female and male C57BL/6J and MRL/MpJ mice. Data points represent individual biological replicates, with averages and standard deviations indicated. Normalized elastic modulus averages and standard deviations were 0.123 +/- 0.065 for C57BL/6J female, 0.160 +/- 0.090 for MRL/MpJ female, 0.145 +/- 0.079 for C57BL/6J male, and 0.238 +/- 0.159 for MRL/MpJ male. Normalized ultimate stress averages and standard deviations were 0.189 +/- 0.056 for C57BL/6J female, 0.310 +/- 0.168 for MRL/MpJ female, 0.250 +/- 0.083 for C57BL/6J male, and 0.349 +/- 0.149 for MRL/MpJ male. Normalized ultimate strain averages and standard deviations were 1.722 +/- 0.334 for C57BL/6J female, 2.177 +/- 0.466 for MRL/MpJ female, 1.826 +/- 0.431 for C57BL/6J male, and 1.838 +/- 0.455

481 for MRL/MpJ male. No statistically significant differences were found between normalized
482 mechanical properties between strains of the same sex or sexes of the same strain.

483

484 Fig. 4. Comparison of heterotopic ossification in injured tendons between C57BL/6J and
485 MRL/MpJ mice. A complete transverse transection was made at the midpoint of the left Achilles
486 tendon in 12-week-old male (square) and female (circle) C57BL/6J (blue) and MRL/MpJ (red)
487 mice (n=5 per strain). Ten weeks after surgery, injured (left) limbs were harvested. (A)
488 Heterotopic ossification was imaged by microCT. Bar represents 1 mm. (B) Total volume of
489 ossified regions within the injured tendon was analyzed. Data points represent individual
490 biological replicates, with averages and standard deviations indicated. Averages and standard
491 deviations were 1.65+/-1.219 for C57BL/6J male, 0.588+/-0.348 for MRL/MpJ male, 1.24+/-
492 0.573 for C57BL/6J male and female and 0.400+/-0.268 mm^3 MRL/MpJ male and female mice.

493

494 Fig. 5. Proteomics analysis of injured tendons of C57BL/6J and MRL/MpJ mice. A complete
495 transverse transection was made at the midpoint of the left Achilles tendon in 12-week-old male
496 C57BL/6J (blue) and MRL/MpJ (red) mice. Four weeks after surgery, injured (left) and
497 contralateral uninjured (right) tendons were harvested, and proteomics analysis was performed.
498 (A) The top 50 upregulated and downregulated proteins in injured tendons samples in both
499 C57BL/6J and MRL/MpJ male mice were well-clustered based on t-test comparisons. (B, C).
500 The top 5 most altered signaling pathways were identified based on IPA analysis of differentially
501 expressed proteins between injured and uninjured tendons of C57BL/6J and MRL/MpJ mice (B),

502 and between C57BL/6J and MRL/MpJ tendons (C). Positive and negative z-scores represent
503 upregulation and downregulation of the corresponding pathway, respectively.

504

505 Supplemental Figure Captions

506 Fig. S1. Representative force-displacement curves for uninjured and injured tendons of both
507 strains and sexes.

508 Fig. S2. Averages and standard deviations of absolute values for cross-sectional area (CSA),
509 stiffness, ultimate load, elastic modulus, ultimate stress, and ultimate strain of uninjured and
510 injured tendons of C57BL/6J female, MRL/MpJ female, C57BL/6J male, and MRL/MpJ male
511 mice.

512

513

514

515

516

517

518

Figure 1

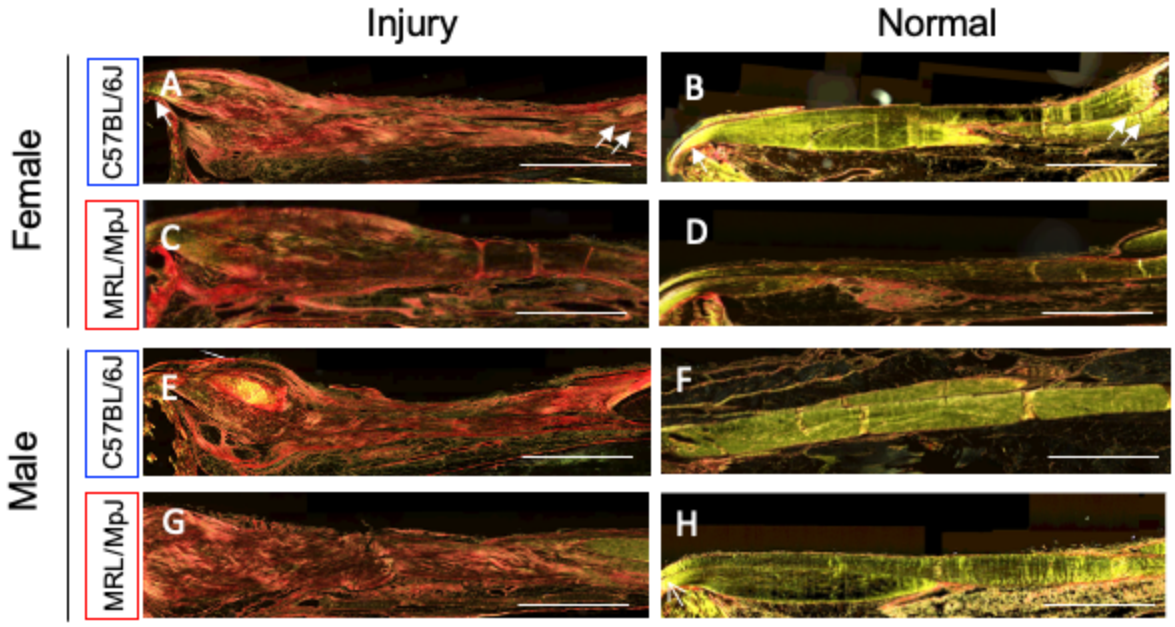
Injury
Normal
Female
Male
C57BL/6J
MRL/MpJ
C57BL/6J
MRL/MpJ
A
B
C
D
E
F
G
H

Figure 2

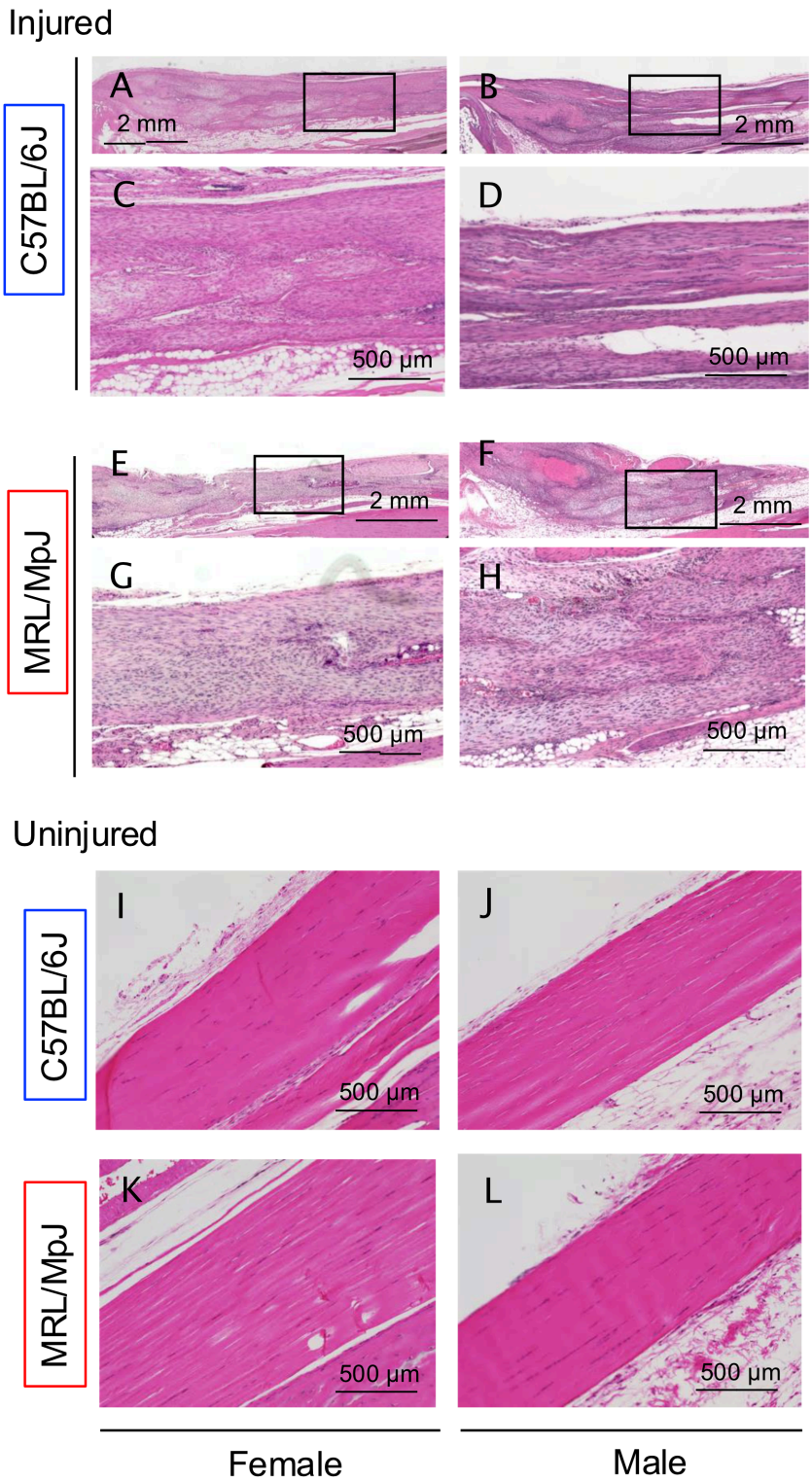
Injured
C57BL/6J
A
2 mm
B
2 mm
C
500 µm
D
500 µm
MRL/MpJ
E
2 mm
F
2 mm
G
500 µm
H
500 µm
Uninjured
C57BL/6J
I
500 µm
J
500 µm
MRL/MpJ
K
500 µm
L
500 µm
Female
Male

Figure 3

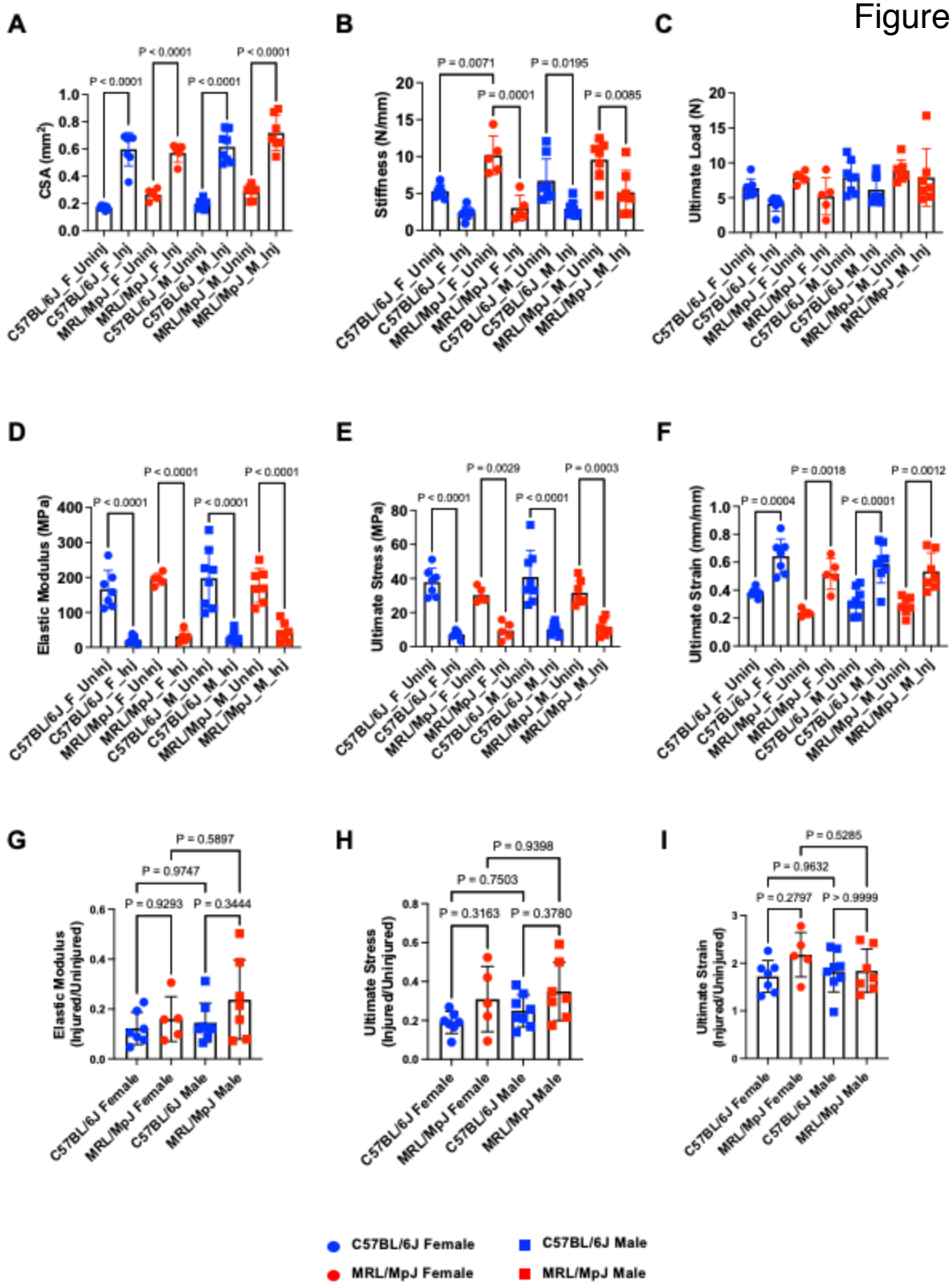
A
CSA (mm²)
P < 0.0001
P < 0.0001
P < 0.0001
P < 0.0001
B
Stiffness (N/mm)
P = 0.0071
P = 0.0001
P = 0.0195
P = 0.0085
C
Ultimate Load (N)
D
Elastic Modulus (MPa)
P < 0.0001
P < 0.0001
P < 0.0001
P < 0.0001
E
Ultimate Stress (MPa)
P < 0.0001
P = 0.0029
P < 0.0001
P = 0.0003
F
Ultimate Strain (mm/mm)
P = 0.0004
P = 0.0018
P < 0.0001
P = 0.0012
G
Elastic Modulus (Injured/Uninjured)
P = 0.5897
P = 0.9747
P = 0.9293
P = 0.3444
H
Ultimate Stress (Injured/Uninjured)
P = 0.9398
P = 0.7503
P = 0.3163
P = 0.3780
I
Ultimate Strain (Injured/Uninjured)
P = 0.5285
P = 0.9632
P = 0.2797
P > 0.9999
C57BL/6J_F_Uninj
C57BL/6J_F_Inj
MRL/MpJ_F_Uninj
MRL/MpJ_F_Inj
C57BL/6J_M_Uninj
C57BL/6J_M_Inj
MRL/MpJ_M_Uninj
MRL/MpJ_M_Inj
C57BL/6J Female
MRL/MpJ Female
C57BL/6J Male
MRL/MpJ Male
C57BL/6J Female
MRL/MpJ Female
C57BL/6J Male
MRL/MpJ Male

Figure 4

A

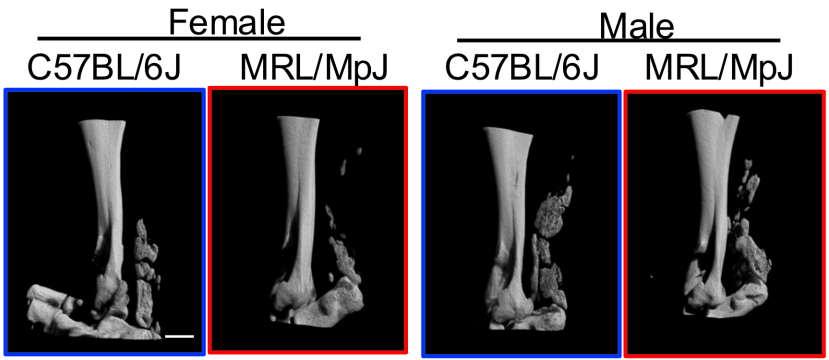
Female
Male
C57BL/6J
MRL/MpJ
C57BL/6J
MRL/MpJ

B

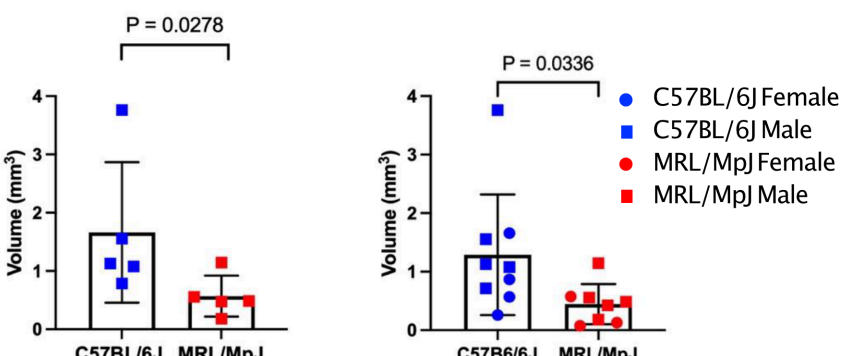
P = 0.0278
Volume (mm³)
0
1
2
3
4
C57BL/6J
MRL/MpJ
P = 0.0336
Volume (mm³)
0
1
2
3
4
C57B6/6J
MRL/MpJ
C57BL/6J Female
C57BL/6J Male
MRL/MpJ Female
MRL/MpJ Male

Figure 5

A T-test comparisons

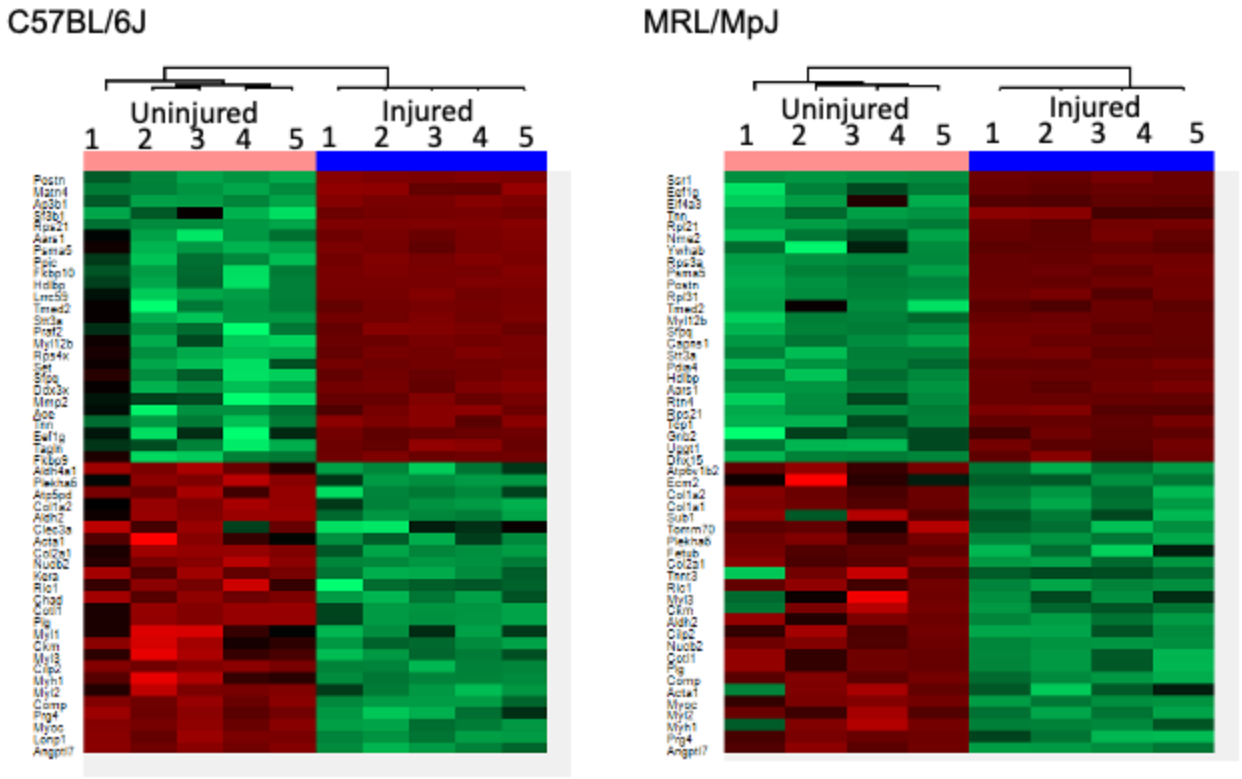

B Injured tendons to uninjured tendons

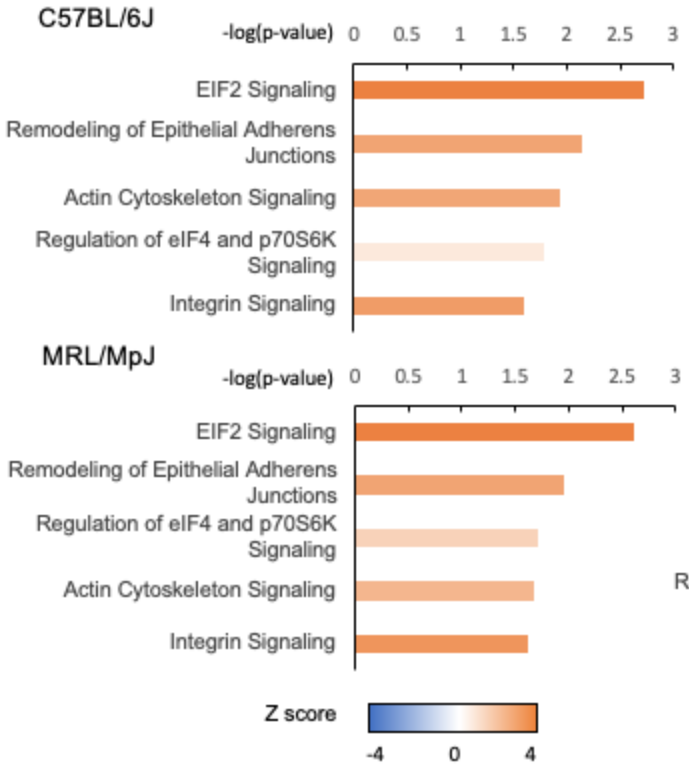

C C57BL/6J to MRL/MpJ

Supplementary Material (Fig. S1 and S2)

Achilles tendons of MRL/MpJ mice show scar-mediated healing after tenotomy

Ningfeng Tang[1], Divya S. Sivalingam[2], Kimberly Wilson[1], Mehari M. Weldemariam[3], Hongying Tian[1], Christoph D. Hart[2], Prishasai Ramnath[2], Jacob Glazier[2], Jie Jiang[1], Natalie Leong[1], Tao Lowe[2,4], Maureen A. Kane[3], Masahiro Iwamoto[1], Catherine K. Kuo[1,2*], Motomi Enomoto-Iwamoto[1*]

*Corresponding Authors

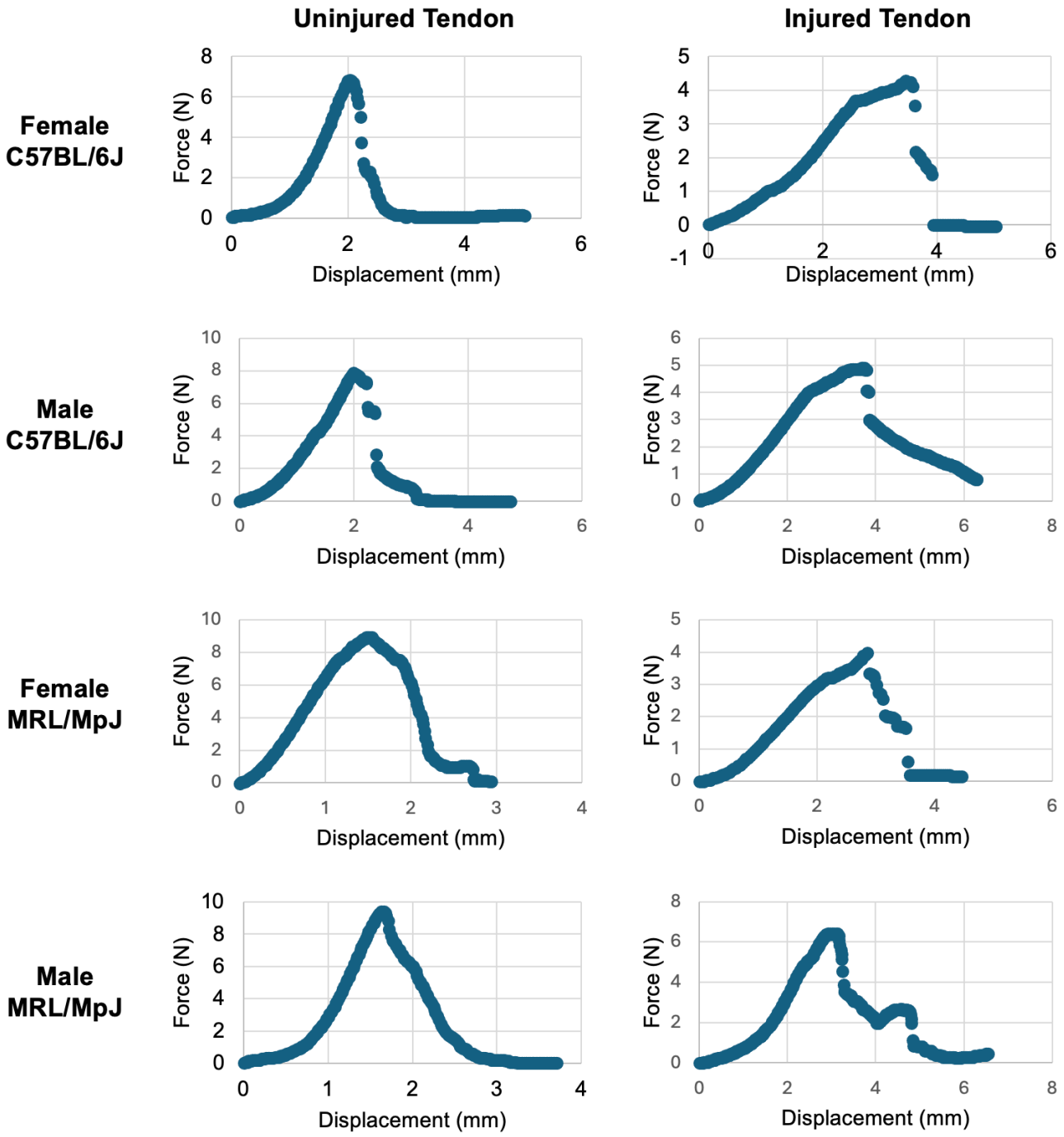

Fig. S1. Representative force-displacement curves for uninjured and injured tendons of both strains and sexes.

Mean ± standard deviation of mechanical properties								
	Female				Male			
	C57BL/6J		MRL/MpJ		C57BL/6J		MRL/MpJ	
	Uninjured	Injured	Uninjured	Injured	Uninjured	Injured	Uninjured	Injured
CSA (mm^2)	0.17 ± 0.01	0.58 ± 0.13	0.27 ± 0.04	0.57 ± 0.07	0.20 ± 0.03	0.62 ± 0.11	0.29 ± 0.05	0.72 ± 0.13
Stiffness (N/mm)	5.32 ± 0.83	2.33 ± 0.85	10.17 ± 2.62	3.04 ± 1.74	6.72 ± 2.96	2.92 ± 1.03	9.57 ± 2.67	5.16 ± 2.96
Ultimate load (N)	6.23 ± 1.28	4.14 ± 1.08	7.90 ± 0.83	5.19 ± 2.67	7.89 ± 2.28	6.15 ± 1.94	8.82 ± 1.57	7.90 ± 4.12
Elastic Modulus (MPa)	169.32 ± 50.35	20.78 ± 10.96	194.92 ± 16.68	31.17 ± 17.50	197.88 ± 84.48	28.79 ± 15.59	176.84 ± 48.43	42.08 ± 28.16
Ultimate Stress (MPa)	37.07 ± 7.91	7.01 ± 2.08	30.21 ± 4.33	9.36 ± 5.08	40.89 ± 15.68	10.21 ± 3.38	31.67 ± 7.16	11.04 ± 4.73
Ultimate Strain (mm/mm)	0.37 ± 0.04	0.64 ± 0.12	0.24 ± 0.02	3.04 ± 0.11	0.32 ± 0.09	0.59 ± 0.14	0.29 ± 0.06	0.53 ± 0.13

Fig. S2. Averages and standard deviations of absolute values for cross-sectional area (CSA), stiffness, ultimate load, elastic modulus, ultimate stress, and ultimate strain of uninjured and injured tendons of C57BL/6J female, MRL/MpJ female, C57BL/6J male, and MRL/MpJ male mice.